

An Active Dominant Mutation of Glycyl-tRNA Synthetase Causes Neuropathy in a Charcot-Marie-Tooth 2D Mouse Model

Kevin L. Seburn,¹ Leslie A. Nangle,² Gregory A. Cox,¹ Paul Schimmel,² and Robert W. Burgess^{1,*}

¹The Jackson Laboratory

600 Main Street

Bar Harbor, Maine 04609

²The Scripps Research Institute

10550 North Torrey Pines Road

La Jolla, California 92037

Summary

Of the many inherited Charcot-Marie-Tooth peripheral neuropathies, type 2D (CMT2D) is caused by dominant point mutations in the gene *GARS*, encoding glycyl tRNA synthetase (GlyRS). Here we report a dominant mutation in *Gars* that causes neuropathy in the mouse. Importantly, both sensory and motor axons are affected, and the dominant phenotype is not caused by a loss of the GlyRS aminoacylation function. Mutant mice have abnormal neuromuscular junction morphology and impaired transmission, reduced nerve conduction velocities, and a loss of large-diameter peripheral axons, without defects in myelination. The mutant GlyRS enzyme retains aminoacylation activity, and a loss-of-function allele, generated by a gene-trap insertion, shows no dominant phenotype in mice. These results indicate that the CMT2D phenotype is caused not by reduction of the canonical GlyRS activity and insufficiencies in protein synthesis, but instead by novel pathogenic roles for the mutant GlyRS that specifically affect peripheral neurons.

Introduction

Charcot-Marie-Tooth neuropathies (CMTs) are inherited disorders of the peripheral nervous system (PNS). As a group, they represent the most common genetic diseases of the PNS, affecting approximately 1 in 2500 people (Skre, 1974). Broadly, the diseases are separated into demyelinating neuropathies (type 1), diagnosed by reduced nerve conduction velocities, and axonal neuropathies (type 2), arising from defects intrinsic to the neuron.

Recent advances in human genetics and mouse models have identified several disease genes and have begun to explain the pathogenic mechanisms of some forms of CMT (Berger et al., 2002; Shy et al., 2002), including genes that act autonomously in Schwann cells to alter myelin and cause type 1 neuropathies (Aguayo et al., 1977; Hayasaka et al., 1993; Roa et al., 1993) and genes involved with the axonal cytoskeleton or vesicle trafficking, causing type 2 neuropathies (Jordanova et al., 2003; Verhoeven et al., 2003).

Interestingly, two forms of CMT are caused by mutations in aminoacyl tRNA synthetases, the enzymes that

covalently link amino acids onto their cognate tRNAs and thereby establish the genetic code relationship between amino acids and the nucleotide triplets that encode them. Mutations in tyrosyl-tRNA synthetase (TyrRS) cause dominant intermediate CMT type C (DICMT-C) (Jordanova et al., 2006). These mutations partially lack enzymatic activity, and the mechanism is proposed to be a haplo-insufficiency, in which protein synthesis is impaired and the resulting peripheral neuropathy presumably reflects the high demands for translation in the peripheral nervous system.

Mutations in the *GARS* gene, encoding glycyl tRNA synthetase (GlyRS), cause CMT2D, a slowly progressive neuropathy that affects primarily the distal extremities (Antonellis et al., 2003). Interestingly, the human *GARS* mutations causing CMT2D are all dominant, are all single amino acid changes, and are not clustered in a particular domain of the enzyme. There is only one gene encoding GlyRS in the mammalian genome, and it gives rise to both the mitochondrial and cytosolic proteins (Mudge et al., 1998; Shiba et al., 1994; Turner et al., 2000). As a dimerizing enzyme with an essential function and no close homologs for redundancy, mutations in *GARS* are similarly good candidates for haploinsufficiency or a dominant-negative mechanism. However, this has not been demonstrated, and an alternative possibility is that the mutant forms of GlyRS are assuming new functions that lead to the loss of peripheral axons.

Though GlyRS aminoacylation activity is required in all cells, CMT2D affects only the peripheral nervous system and begins only after young adulthood. Motor neurons are affected in all cases, but the involvement of sensory neurons is variable and not well defined clinically. Thus CMT2D is also diagnosed as distal spinal muscular atrophy V (SMA-DV) (Antonellis et al., 2003; Del Bo et al., 2006; Dubourg et al., 2006; Sambuughin et al., 1998; Sivakumar et al., 2005), and the cause of the variable presentation is unknown.

We have identified a mouse model of CMT2D, developed through the positional cloning of a mutation causing overt neuromuscular dysfunction. The mutation is an amino acid alteration in *Gars*, the mouse ortholog of the CMT2D gene *GARS*. Phenotypically, the mice have a severe axonal neuropathy of both sensory and motor axons. Biochemical and genetic analyses indicate that the phenotype is not caused by a haplo-insufficiency or a dominant-negative loss-of-function mechanism, thus the mutant protein must be assuming a novel pathogenic role in peripheral neurons.

Results

Identification of a *Gars* Mutation in Mice

We have identified a mouse mutation causing overt neuromuscular dysfunction by 3 weeks of age (see video at <http://www.jax.org/media/burgess/burgess.html>) and dramatically shortening average life span. The mutation, designated *Nmf249*, was identified in the Neurosciences Mutagenesis Facility at The Jackson Laboratory in 2004 (www.jax.org/nmf/). The inheritance pattern indicated a

*Correspondence: robert.burgess@jax.org

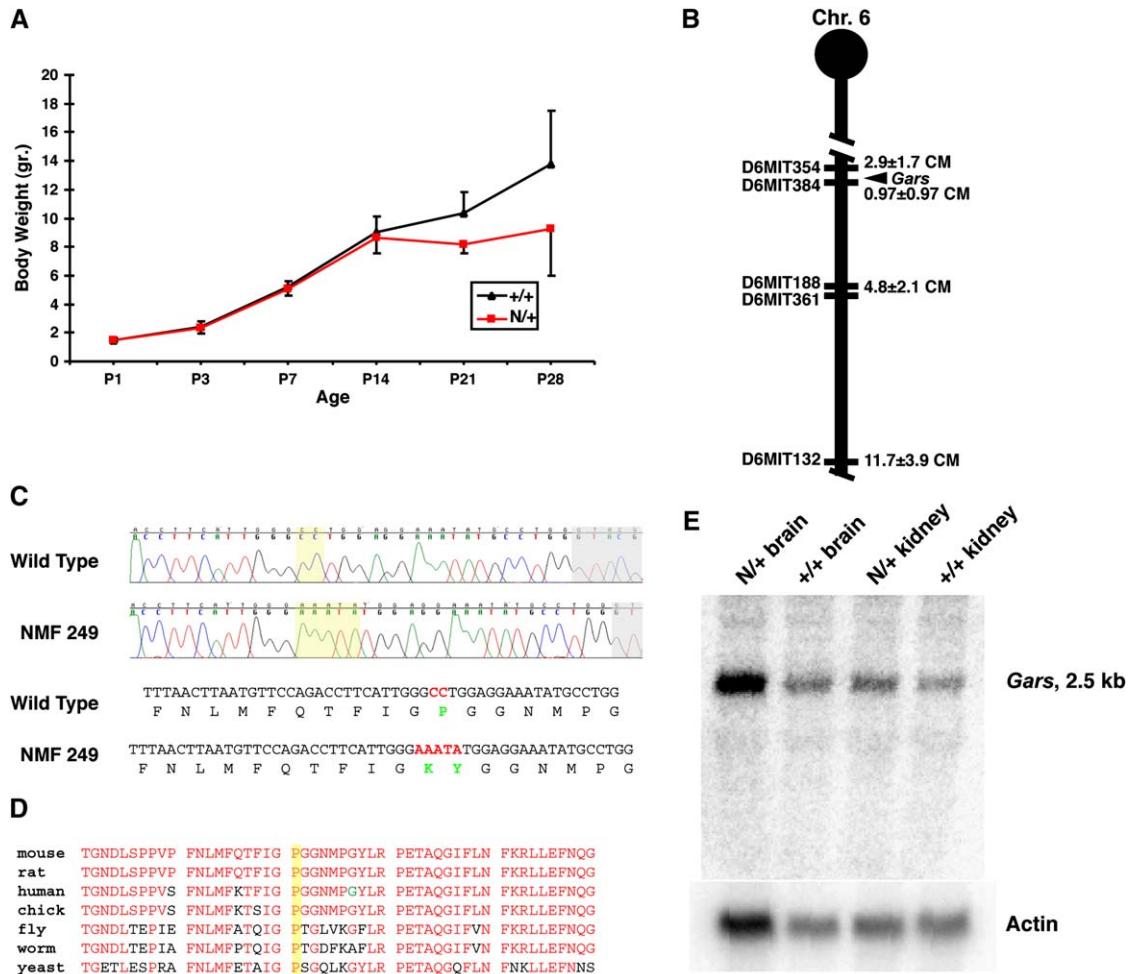


Figure 1. Positional Cloning of *Nmf249*

(A) Affected mice were scored based upon overt neuromuscular dysfunction and significantly reduced body weight, evident by 3 weeks of age ($p < 0.0001$). Body weights \pm SD are shown for affected and unaffected littermates from nine different matings ($n = 6$ –13 mice per time point). (B) Analysis of 103 N2 mice defined the genetic interval containing the mutation as 1.9 mb between *D6Mit354* and *D6Mit384*, which contains the *Gars* gene. (C) Sequencing *Gars* revealed a change of CC to AAATA (highlighted in the chromatogram) in the portion of the transcript encoded by exon 7, changing proline 278 to a lysine and tyrosine. The beginning of intron 7 is shaded gray. (D) The altered proline is highly conserved and is only six amino acids from a glycine altered in one allele of *GARS* identified in human CMT2D patients (green G in human sequence). Conserved amino acids are in red; the altered proline is highlighted yellow. (E) The change in the *Gars* coding sequence does not alter mRNA expression levels based on Northern analysis using β -actin as a loading standard.

dominant mutation, with 23/56 offspring affected when the original carrier was bred to wild-type C57BL/6J (B6) males (see [Experimental Procedures](#)). The mutation is most often lethal by 6–8 weeks of age, with only 10 of 254 affected mice surviving longer than 6 months in an inbred B6 colony.

The mutation arose in a B6 background and was mapped in an N2 backcross to BALB/cByJ (BALB). Affected mice were scored based upon smaller size ([Figure 1A](#)) and the overt neuromuscular phenotype. No change in the mutant phenotype was observed in B6/BALB F1 mice, suggesting that the phenotype is not modified by loci in the BALB genetic background. A genome scan was performed on 16 affected and 11 unaffected N2 mice, and linkage was established with *D6Mit188* at 32.5 cM on chromosome 6. Analysis of 76 additional N2 recombinants narrowed the interval to 1.9 mb be-

tween *D6Mit354* and *D6Mit384* ([Figure 1B](#)), a region with shared synteny to human chromosome 7p15.

This interval contains *Gars*, the mouse ortholog of the CMT2D gene, *GARS*, in humans. *Gars* is a 17 exon gene encoding a 729 amino acid protein. Given the neuromuscular phenotype of *Nmf249*, we sequenced the *Gars* cDNA in affected mice and identified a change in the open reading frame. A replacement of CC with AAATA changes the proline at residue 278 to tyrosine and lysine ([Figure 1C](#)) without affecting the rest of the open reading frame. Proline 278 is conserved throughout eukaryotic phylogeny ([Figure 1D](#)), extending even to bacteria. The amino acid is near the catalytic domain 2 of the protein and is close in the primary sequence to an amino acid affected in one human disease allele. The mutation does not affect *Gars* mRNA levels, as shown by Northern analysis ([Figure 1E](#)).

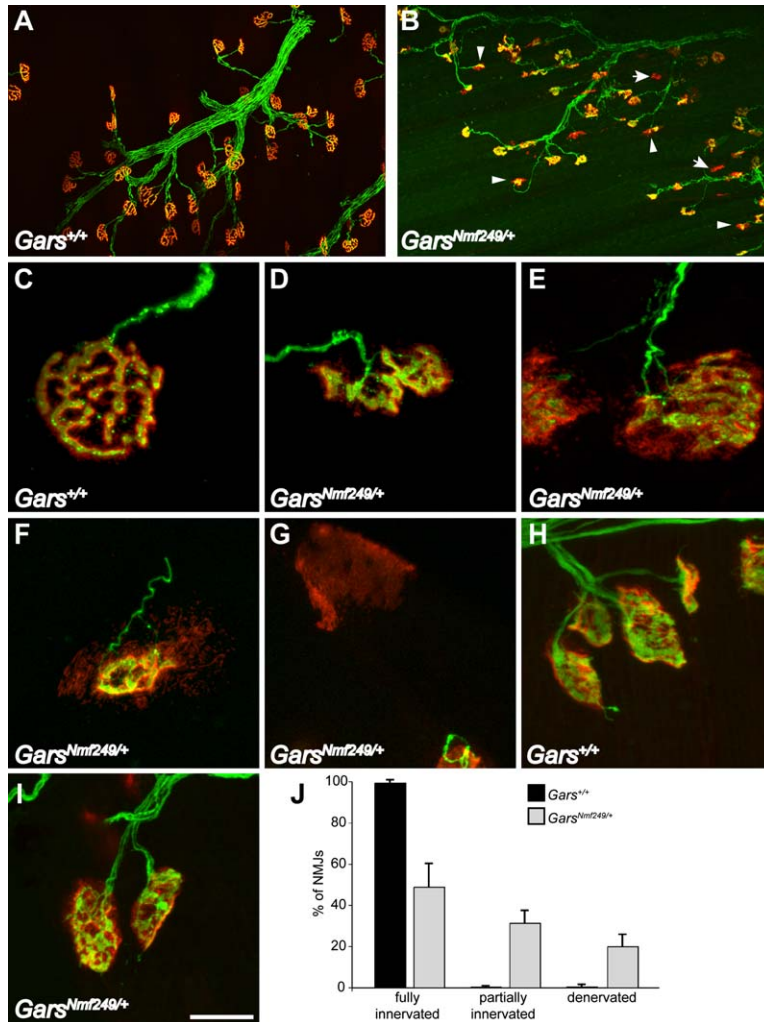


Figure 2. Neuromuscular Junction Morphology and Denervation in *Gars*^{Nmf249/+} Mice

(A) Control neuromuscular junctions (NMJs) in the gastrocnemius muscle of P36–P37 mice show normal branching and mature morphology, with the motor nerve terminal (green) completely overlapping the acetylcholine receptors (AChRs) on the muscle (red). (B) In *Gars*^{Nmf249/+} mice, the motor neurons still branch within the muscle; however, NMJs have an abnormal morphology, and numerous partially innervated (arrowheads) and completely denervated (arrows) postsynaptic sites are seen. (C) At higher magnification, the nerve terminal is directly above the AChRs on the muscle, and the synapse has assumed a “pretzel-like” morphology in control mice. (D) NMJs from *Gars*^{Nmf249/+} mice never achieve a normal morphology, and a “best case” junction is shown. (E) Many junctions show regions of postsynaptic specialization that are not overlain by the nerve terminal. (F) In some cases, only a small portion of the postsynaptic receptor field is covered by the nerve terminal. Note the small diameter of the axon. (G) Receptor fields with no associated nerve are also evident. The abnormalities in innervation at P36–P37 are degenerative, as no differences are seen between control (H) and *Gars*^{Nmf249/+} (I) NMJs at P7. (J) Quantification of the NMJs at P36–P37 revealed that in *Gars*^{Nmf249/+} gastrocnemius muscles, only 48.8% ± 11.4% of the NMJs were completely overlapped by a nerve terminal (as in [D]), while 31.3% ± 6.1% were partially overlapped (as in [E] and [F]), and 19.9% ± 5.9% had no nerve in close proximity (as in [G]). The scale bar in (I) represents 172 μm for (A) and (B) and 14 μm for (C)–(I). Values in (J) are mean ± SD.

Neuromuscular Junction Defects in *Gars*^{Nmf249/+} Mice

Since CMT2D causes a distally accentuated loss of motor axons, we examined the neuromuscular junctions of affected mice. In mature control mice, motor neurons entered the muscle and branched, with each muscle fiber contacted by a single motor nerve terminal. The nerve terminal completely overlapped the postsynaptic receptor field on the muscle (Figures 2A and 2C). In *Gars*^{Nmf249/+} mice, the general pattern of innervation was comparable to controls; nerves entered the muscle and branched. However, by P36–P37, many partially innervated and completely denervated junctions were apparent (Figures 2B and 2D–2G). This process was degenerative, since NMJs in control and mutant P7 mice were indistinguishable (Figures 2H and 2I). The occupancy (the extent of overlap between the pre- and postsynaptic structures) of NMJs was determined at each age. At P7, NMJs were fully occupied in both control and *Gars*^{Nmf249/+} mice (99.0% ± 1.2% and 99.4% ± 0.5%, respectively, n = 5 mutant and 5 littermate control mice, 100 NMJs examined per muscle). However, at P36–P37 the control mice maintained full occupancy (99.25% ± 1.5%), while *Gars*^{Nmf249/+} mice showed 31.3% ± 6.1% partially occupied and 19.9% ± 5.9% de-

nervated NMJs (Figure 2J, n = 4 mutant and 4 littermate control mice).

The results shown in Figure 2 and reported above were obtained in the gastrocnemius muscle, and similar results were obtained in the neighboring soleus and plantaris (data not shown). Interestingly however, a much milder phenotype was seen in the triangularis sterni, an axial muscle on the medial ribcage (see Figure S1 in the Supplemental Data available online), in which 92.25% ± 2.0% of NMJs were fully innervated and 7.5% ± 1.7% were partially innervated. In sum, these results indicate a severe degenerative process in the motor nerve terminals and are consistent with length-dependence pathology, with more distal muscles of the hind limb having a more severe neuropathy.

Functional analysis of muscle contractile properties evoked by tetanic nerve stimulation revealed failure in production and maintenance of muscle force in 8-week-old mice. The failure to maintain force corresponded to decreased electromyogram amplitude, suggesting synaptic transmission failure at higher frequencies (Figures 3A and 3B). Although analysis revealed reduced muscle weights (Figure S2), even when normalized for body weight, this was attributable to smaller fiber size, and no pathological changes were seen

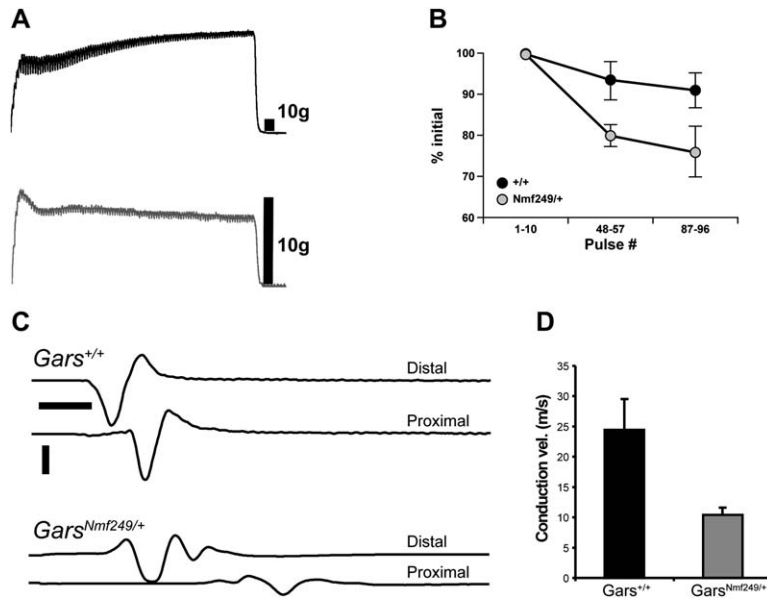


Figure 3. Muscle Contractile Properties and Nerve Conduction in *Gars^{Nmf249/+}* Mice

(A) The medial gastrocnemius muscle was assayed for tetanic force generation with 80 Hz stimulation of the nerve. Control muscles show tetanic fusion and maintain force for 1.2 s of stimulation (top trace). Mutant muscles show tetanic fusion, although with much less force generated, but fail to maintain force (bottom, gray trace).

(B) The failure to maintain force corresponds to a significant decrement in the integrated electromyogram (EMG) amplitude ($p < 0.01$ at pulses 48–57 and pulses 87–96). For (A) and (B), four *Gars^{Nmf249/+}* mice (mean age 56 ± 20 days) and four *Gars^{+/+}* mice (mean age 55 ± 12 days) were analyzed.

(C) Electromyogram traces showing latencies in response to distal and proximal nerve stimulation revealed a decreased compound muscle action potential amplitude and increased latency in the *Gars^{Nmf249/+}* mice. The scale bars correspond to 1 ms (horizontal) and 1 mV (vertical).

(D) Quantification of the increased distal latency indicated a significant decrease in nerve conduction velocity ($p < 0.01$). Values in (B) and (D) are means \pm SD.

histologically, nor was a reduction in fiber number observed in young animals, although the kinetics of the isometric twitch contractions were slowed.

Nerve conduction velocities (NCVs) were also decreased by 60% in the affected mice, falling from 24.4 ± 5.1 m/s in control animals to 10.4 ± 1.2 ($p < 0.01$) in the sciatic nerve of *Gars^{Nmf249/+}* mice (Figures 3C and 3D) (three mutant and three control animals measured at P34). Although the defects in distal motor-axon morphology and synaptic connectivity with minimal muscle pathology are consistent with an axonal/type 2 neuropathy, the reduced nerve conduction velocity is clinically diagnostic of demyelinating/type 1 CMTs and has been reported as unaffected or moderately reduced in CMT2D patients (Del Bo et al., 2006; Ionasescu et al., 1996; Sivakumar et al., 2005).

Reduced Axon Diameter without Myelination Defects in *Gars^{Nmf249/+}* Sciatic Nerves

We investigated possible causes of reduced NCV in the *Gars^{Nmf249/+}* mice, including decreased axonal diameter and demyelination in the peripheral nerve. We also examined the distance between nodes of Ranvier on teased axons, since shortened internodal distances (INDs) decrease the efficiency of saltatory conduction and have been reported as a cause of reduced NCV in periaxin null mice (Court et al., 2004).

The sciatic nerve was examined at P7, and the nerves from control and mutant animals were indistinguishable by histological staining (Figures 4A and 4B). Importantly, the largest myelinated axons of the *Gars^{Nmf249/+}* nerves were equivalent in size to the largest axons of control nerves (Figures 4C). However, a small but significant shift in the distribution of axon diameters ($p < 0.001$, K-S test) was found, including a population of smaller-diameter axons with comparatively thick myelin in the mutant nerves (circled, Figure 4C). The distribution of myelin thicknesses was unchanged in mutant versus

control samples at P7 ($p > 0.1$, K-S test). However, the G-ratio (total diameter including myelin/axon diameter) was also significantly decreased (0.67 ± 0.10 in control versus 0.63 ± 0.13 in mutant mice, $p < 0.001$, K-S test), consistent with normal myelination and reduced axon diameter. This suggests that mild axonal atrophy predominantly affecting larger axons may already be present at P7.

By P35, the mean axonal diameter of myelinated fibers was further decreased in mutant nerves (Figures 4D–4H). A complete absence of large-diameter axons was evident. An additional eight *Gars^{Nmf249/+}* and six *Gars^{+/+}* sciatic nerves, ages P21–P37, were examined by Toluidine blue histology and were qualitatively like those of the P35 mice quantified by TEM for Figure 4F, with large-diameter axons clearly missing from all the *Gars^{Nmf249/+}* nerves. Degenerating axons were also observed in nerves from *Gars^{Nmf249/+}* mice (Figures 4I and 4J), with 18 degenerating axonal profiles observed in the 448 mutant axons examined by TEM, while no such profiles were seen in 223 wild-type axons. Degenerating axons were defined as those with no visible axoplasm, surrounded by an intact myelin sheath and basal lamina. The preferential loss of large axons is consistent with the altered muscle contraction kinetics (Figure S2), as these axons innervate large, fast-contracting motor units.

The remaining axons were still myelinated, and no evidence of demyelination, such as “onion bulb” pathology or thinly myelinated axons (Suter and Scherer, 2003), was observed. The G-ratio determined from P35 TEM images collected above actually decreased (0.57 ± 0.11 control versus 0.50 ± 0.12 mutant, $p < 0.001$, K-S test). This can be explained by the degeneration of large-diameter axons while maintaining a relatively normal range of myelin thicknesses (Figure 4F) and is inconsistent with a demyelinating neuropathy.

Internodal distances (INDs) were not significantly reduced in mutant mice (519 ± 36 versus 475 ± 41 μ m

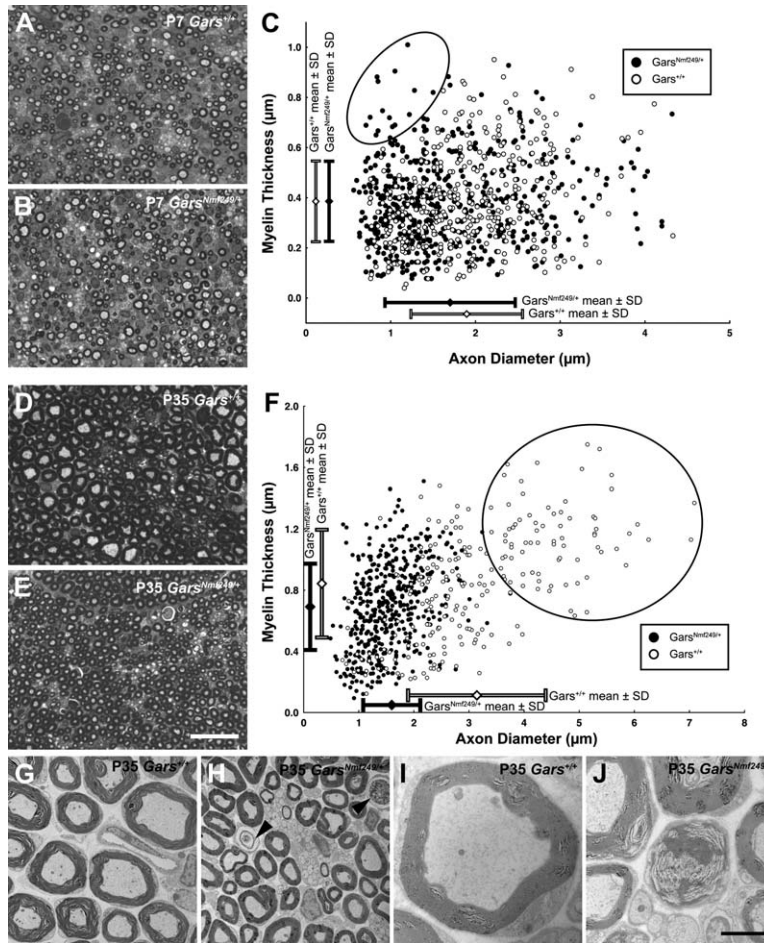


Figure 4. Loss of Large-Diameter Peripheral Axons without Defects in Myelination

At P7, sciatic nerves from *Gars*^{+/+} mice (A) and *Gars*^{*Nmf249/+*} mice (B) show no obvious pathology. (C) However, the distribution of axonal diameters is slightly but significantly shifted in the mutant nerves, with a population of small, presumably atrophic axons already evident at this age (circled in Figure 5C). Myelin thickness is not significantly different ($p > 0.1$, K-S test). A total of 516 axons from four *Gars*^{*Nmf249/+*} mice and 392 axons from three *Gars*^{+/+} mice were measured by transmission electron microscopy (TEM) in these analyses. At P35, control mice have large-diameter axons in the sciatic nerve (D), circled in [F]), while *Gars*^{*Nmf249/+*} mice completely lack large-diameter axons (E). (F) The mean axonal diameter is decreased from 3.13 ± 1.27 in *Gars*^{+/+} mice to 1.57 ± 0.54 in *Gars*^{*Nmf249/+*} mice ($p = 0.0002$, K-S test). The maximum size of axons is reduced from 7.1 to $3.8 \mu\text{m}$, and consistent with the loss of large-diameter axons, the distribution of myelin thicknesses is reduced in mutant mice from a mean of 0.84 ± 0.36 to 0.69 ± 0.28 ($p < 0.001$, K-S test, 223 axons from three P35 *Gars*^{+/+} mice and 448 axons from three P35 *Gars*^{*Nmf249/+*} mice were analyzed by TEM for [F]). TEM analysis of *Gars*^{+/+} (G) and *Gars*^{*Nmf249/+*} (H) sciatic nerves revealed no hallmarks of demyelination/remyelination. No degenerating axons were seen in control mice (I), while axon profiles wrapped by a single Schwann Cell and basal lamina, but lacking clear axoplasm, were observed in *Gars*^{*Nmf249/+*} nerves (arrowheads in [H] and [J]). Scale bar in (E) is $30 \mu\text{m}$ for (A), (B), (D), and (E), and bar in (I) is $6.5 \mu\text{m}$ for (G) and (H) and $1.5 \mu\text{m}$ for (I) and (J).

for *Gars*^{+/+} and *Gars*^{*Nmf249/+*} mice, respectively, $p = 0.24$, $n = 3$ mice, 234 INDs measured for *Gars*^{+/+} mice, and 3 mice, 344 INDs measured for *Gars*^{*Nmf249/+*} mice, age P35). A trend toward smaller INDs is anticipated with the loss of large-diameter axons. Thus the absence of fast-conducting, large-diameter axons from peripheral nerves explains the reduced NCV, with no evidence for contribution from demyelination or decreased internodal distances.

Slowly Progressing Sensory and Motor Peripheral Axon Loss in *Gars*^{*Nmf249/+*} Mice

We examined sensory involvement in the mouse model of CMT2D by counting axons in the motor and sensory branches of the femoral nerve (Scherer et al., 2005) at P7–P8 and P32–P35 ($n = 1$ mutant and control littermate pair at P7, 2 mutant and control littermate pairs at P8; P7 and P8 numbers were pooled for each genotype). No reduction in myelinated axon number was seen at P7–P8 in either motor or sensory nerves (Figures 5A–5E). However, by P32 a significant decrease in both motor (23% [$p < 0.01$]) and sensory (19% [$p < 0.01$]) axon number was seen (Figures 5F–5J). Four P32 *Gars*^{*Nmf249/+*} mice, one P32 *Gars*^{+/+} littermate, and three P35 C57BL/6J control mice were analyzed. As in the sciatic nerve, the axons missing were the largest-diameter fibers, and the combination of smaller axon diameter and reduced number resulted in a strikingly smaller nerve. Therefore,

the *Gars*^{*Nmf249/+*} model of CMT2D has clear sensory axon involvement. Furthermore, the number of unmyelinated axons in control and mutant femoral motor branches of the P32 mice was unchanged (331 ± 13 and 383 ± 91 , $p = 0.34$), suggesting that the myelinated axons are truly lost and not atrophied or demyelinated.

Most of the affected mice die between 5 and 8 weeks of age, but, approximately 4% of the animals survive 6 months or more in the B6 genetic background. Little overt progression in the severity of neuromuscular dysfunction is seen in these mice, even when aged to 1 year. Quantification of axons in the femoral nerves from 52- to 61-week-old mice revealed modest but significant progression in the motor axon loss (an additional 12% of axons were lost, $p < 0.01$) with less progression in axon loss in sensory nerves (an additional 4% loss, $p = 0.056$) (Figure 5F). Motor branches from three *Gars*^{*Nmf249/+*} and four *Gars*^{+/+} mice and sensory branches from four *Gars*^{*Nmf249/+*} and four *Gars*^{+/+} littermates were counted. Thus, most of the axon loss in the *Gars*^{*Nmf249/+*} mice occurs by 1 month of age, and mice that do not succumb to the initial insult exhibit only a modest additional decrease in axon number at 1 year.

The axonal phenotype is more pronounced distally. Examination of the femoral motor nerve and the fifth lumbar ventral root (L5), both isolated from the same mice at P34, revealed that the femoral nerve lost 28%

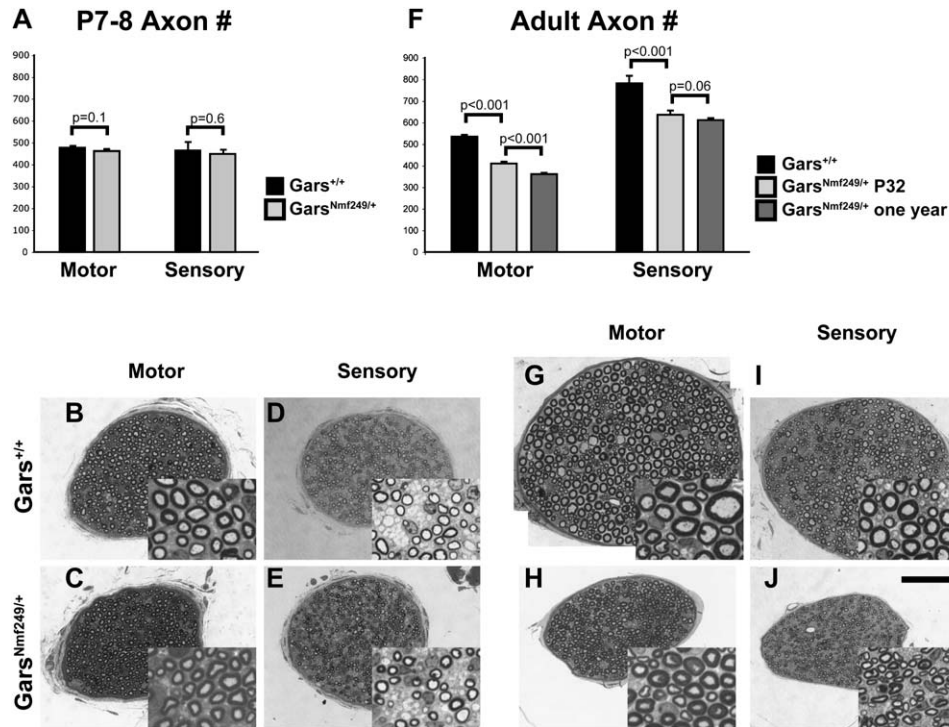


Figure 5. Motor and Sensory Axon Loss

(A) Myelinated axons from the motor and sensory branches of the femoral nerve were counted at P7–P8 in *Gars*^{+/+} and *Gars*^{Nmf249/+} mice. No significant change in axon number was found in either the sensory or motor branch of the nerve. Like the sciatic, femoral motor nerves from control (B) and mutant (C) were indistinguishable, as were sensory branches (D and E). However, at P32–P35 a significant decrease in the number of myelinated sensory and motor axons was found (F). Axons in the motor branch decreased from 781 ± 36 in control mice to 636 ± 20 in *Gars*^{Nmf249/+} nerves ($p < 0.001$). As in the sciatic nerve, large-diameter axons were lost (G–J). In mice greater than 1 year of age (F), significant additional loss of axons was evident in the motor branch (361 ± 6 , $p < 0.001$), but not in the sensory branch (611 ± 7 , $p = 0.06$). No differences in axon number at 1 year of age were seen in control nerves (539 ± 7 motor and 793 ± 10 sensory). Scale bar in (J) is $50 \mu\text{m}$ for (B)–(E) and (G)–(J). Insets are $30 \times 22.5 \mu\text{m}$. The values in (A) and (F) are means of axon number in each nerve \pm SD.

of its myelinated axons (530 ± 16 in control versus 382 ± 30 in mutant samples, $n = 3$ mice of each genotype), while there was no change in the axon number in the L5 root (963 ± 130 in control versus 1020 ± 28 in mutant roots). Similarly, no pathology was evident in the spinal cord of mutant animals (data not shown, $n = 5$ examined at P24 and $n = 4$ examined at P36–P37). Thus the neuropathy progresses from distal to proximal, with a loss of axons in distal nerve branches and no loss of axons in ventral roots, or death of cell bodies in the spinal cord.

Muscles from the older mice showed evidence of atrophy and long-term denervation and reinnervation (Figure S3). These changes included fibrosis and hypertrophic, atrophic, and regenerated muscle fibers. Muscle fibers were also lost, and grouping of muscle fiber types caused by denervation and compensatory terminal sprouting of the remaining motor neurons was evident in the mutant muscles.

To test whether a hybrid genetic background could improve survival, a B6 \times BALB F1 mouse was mated to CAST/EiJ. The resulting hybrids carrying the *Gars*^{Nmf249} mutation were still overtly affected with a similar age of onset. However, more mice survived beyond 8 weeks (>90%), and these mice could be bred by standard practices. Interestingly, no *Gars*^{Nmf249/Nmf249} homozygous mice were identified at birth, suggesting

they are embryonic lethal (20 offspring genotyped from 4 litters, χ^2 value = 0.035).

Gars^{Nmf249} Is Not a Loss-of-Function Allele

The more severe phenotype (embryonic lethality) of homozygous *Gars*^{Nmf249/Nmf249} mice is consistent with the anticipated loss-of-function phenotype but could also be explained by an increased dose of a toxic gain-of-function protein. Furthermore, the P278KY mutation is near one human allele (G240R, see Figure 1D) immediately before domain 2 of the catalytic portion of the protein. However, other reported human alleles are spread across the peptide sequence (E71G, L129P, D500N, and G526R) (Antonellis et al., 2003; Del Bo et al., 2006). These amino acids do not cluster to a functional domain such as the catalytic or anticodon recognition domains, raising the question of whether the disease is correlated with changes in GlyRS enzyme activity.

To address the genetic mechanism of the *Gars*^{Nmf249/+} mutation, we examined an unambiguous loss-of-function allele. This allele is the result of a gene-trap insertion (XM256) in the second intron of the 17 exon *Gars* gene (Skarnes et al., 1995). In mRNA samples isolated from brain and kidney, *Gars*^{XM256/+} mice had expression levels of 59% and 54%, respectively, compared to controls ($n = 3$ each genotype, littermates, age P44). Thus

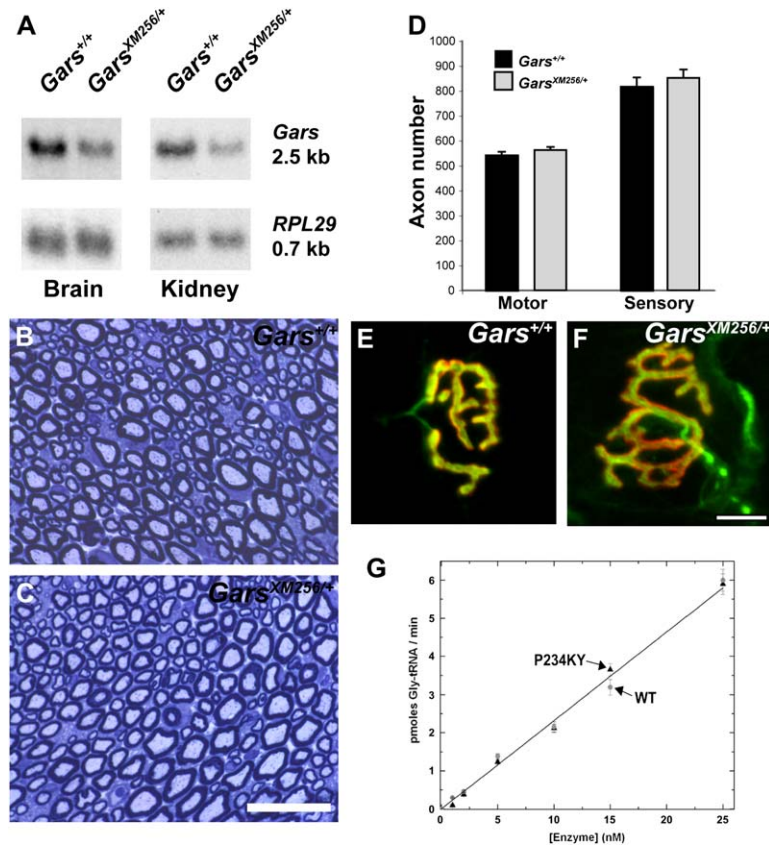


Figure 6. Dominant *Gars* Mutation Is Not a Loss-of-Function Mutation

The genetic mechanism of dominant *Gars* mutations was examined by comparison to a gene-trap allele of *Gars* (*Gars*^{XM256}) that intercepts transcripts after exon 2. (A) The XM256 insertion effectively reduced mRNA levels by Northern analysis using a cDNA probe that is downstream of exon 2. Expression of *Gars* was quantified using phosphor-imager densitometry and compared hybridization intensity of a standard (*RPL29*) applied to the same blots; representative adjacent lanes are shown. Despite the loss of *Gars* mRNA, the sciatic nerves of *Gars*^{+/+} littermate control (B) and *Gars*^{XM256/+} mice (C) are indistinguishable, with no loss of large-diameter axons and no evidence of degenerating axons in the gene-trap mice. (D) The femoral nerves showed no decrease in axon number in either the sensory or motor branch, and the neuromuscular junctions of control (E) and *Gars*^{XM256/+} mice (F) were indistinguishable, indicating that the abnormal post-synaptic differentiation observed in the *Gars*^{Nmf249/+} mice was not present in the gene-trap mice. No denervated or partially denervated junctions were seen. All analyses in (B)–(G) were done on three *Gars*^{XM256/+} mice and three *Gars*^{+/+} littermates, age P44. (G) Mutant and wild-type recombinant GlyRS protein was assayed for initial rates of aminoacylation (pmoles Gly-tRNA/min \pm SD for each enzyme concentration tested, wt [circles], or P234KY [triangles]). No decrease in enzymatic activity was seen in the mutant form of the protein. Each point represents the mean of six trials. The scale bar in (C) represents 30 μ m, the bar in (F) represents 11 μ m. The values in (B) are reported \pm SD.

the gene-trap insertion effectively reduced *Gars* expression (Figure 6A). These results were confirmed by quantitative PCR analysis, which indicated a 1.8 ± 0.4 -fold reduction in *Gars* expression (data not shown, see Experimental Procedures). Therefore, this allele is a loss-of-function allele at the mRNA level. Furthermore, the gene-trap allele is also embryonic lethal, with no *Gars*^{XM256/XM256} homozygotes evident at birth in 18 pups from five litters ($\chi^2 = 0.04$), again consistent with the anticipated loss-of-function phenotype for this gene and suggesting that little if any wild-type splicing was still present.

Despite the loss of *Gars* expression, this allele showed no dominant phenotype. The sciatic nerves of *Gars*^{XM256/+} mice contained large-diameter axons and were histologically indistinguishable from littermate controls (Figures 6B and 6C). Similarly, there was no loss of axons in either the motor or sensory branch of the femoral nerve (Figure 6D), and neuromuscular junctions had mature morphology with no evidence of denervated synapses (Figures 6E and 6F). Nerve conduction velocities in *Gars*^{XM256/+} mice were not different than those in wild-type littermates (30.4 ± 3.8 m/s versus 30.6 ± 2.7 m/s in *Gars*^{+/+} and *Gars*^{XM256/+} mice, respectively, $n = 3$ mice each genotype, average age P35 \pm 8.7), and the NMJs in the lateral gastrocnemius showed complete occupancy ($98.5\% \pm 1.3\%$ fully

innervated NMJs, $n = 4$ *Gars*^{XM256/+} mice, average age P34 \pm 7.5).

To determine whether the P to KY mutation affected GlyRS enzymatic activity, the change was introduced in the human *GARS* coding sequence (Figure S4). Wild-type and P234KY human GlyRS were overexpressed in *E. coli*, purified to near-homogeneity, and assayed for initial rates of aminoacylation (time points during the first 4 min of the reaction) at enzyme concentrations of 1, 2, 5, 10, 15, and 25 nM. For both wild-type and mutant enzyme, the initial rates showed a strictly linear dependence on total enzyme concentration, with both sets of initial rates scattering about the same line (Figure 6G). Because the initial rates for both enzymes were the same over a 25-fold range of concentration, we conclude that the P234KY substitution does not disrupt the active site and that the mutant enzyme is fully active. This finding suggests that the mutant phenotype does not arise from haplo-insufficiency or a dominant-negative pathogenic mechanism.

Despite the normal activity of the P234KY GlyRS, the *Gars*^{Nmf249} allele could still be causing a loss-of-function phenotype through mechanisms such as protein instability or reduced efficiency of folding. Interestingly, when *Gars*^{Nmf249/+} and *Gars*^{XM256/+} mice were mated, no compound heterozygous offspring were identified at birth in 28 mice from five litters (χ^2 value = 0.02).

This failure to complement could indicate a loss of function in *Nmf249* or it could indicate that the wild-type allele has some ability to compensate for or compete with the mutant protein in a pathogenic gain of function. However, for a loss-of-function or dominant-negative mechanism to account for the dominant CMT2D-like phenotype, the GlyRS activity in *Gars*^{*Nmf249*/+} would have to be reduced significantly more than in *Gars*^{*XM256*/+}, which showed no phenotype. To assess this, GlyRS activity was assayed directly from brain homogenates of *Gars*^{+/+}, *Gars*^{*Nmf249*/+}, and *Gars*^{*XM256*/+} mice. The activity of alanyl-tRNA synthetase (AlaRS) was used as an internal standard for each sample, and the ratios of GlyRS to AlaRS activity were determined and normalized to the control values, defined as 100%. Ratios of GlyRS/AlaRS activities of 100 ± 49 , 63 ± 14 , and 29 ± 5 were obtained for *Gars*^{+/+}, *Gars*^{*Nmf249*/+}, and *Gars*^{*XM256*/+}, respectively. While *Gars*^{*Nmf249*/+} tissue showed only an insignificant decrease in activity compared to control ($p = 0.14$), it retained significantly more activity than *Gars*^{*XM256*/+} tissue ($p = 0.006$). The assay was performed with $n = 5$ *Gars*^{*Nmf249*/+} mice, $n = 3$ *Gars*^{*XM256*/+} mice, and $n = 4$ control mice.

Because the *Gars*^{*XM256*} mice represent a loss-of-function allele, have less GlyRS activity as heterozygotes than *Gars*^{*Nmf249*/+} mice, and have no dominant phenotype and because the recombinant P234KY enzyme retains normal kinetics and activity, we conclude that the *Gars*^{*Nmf249*} allele causes peripheral neuropathy because the mutant GlyRS protein assumes a pathogenic function, and not because of a loss of GlyRS activity.

Discussion

A Mouse Model of CMT2D

We have quantitatively analyzed the first animal model of CMT2D. As in the human patients, the mutation is dominant and causes an amino acid substitution, not a truncation or null allele. The mice demonstrate clear distal motor neuropathy with defects in synaptic connectivity at the NMJ and denervation pathology in the muscle. In addition, large-diameter axons are lost from both motor and sensory peripheral nerves, causing reduced nerve conduction velocities without contributing defects in myelination or internodal distances. Furthermore, the mice show distally accentuated and length-dependent axon loss, with no observed pathology in the spinal cord. Based on these genetic and phenotypic analyses, this mutation creates a valid model of CMT2D for use in future mechanistic studies.

The nerve conduction velocities in the mouse are decreased dramatically (60%), while human patients often show no decrease in conduction velocity (Ionasescu et al., 1996), or only a modest decrease in the lower limbs, with values in the peroneal nerve as low as 34.5 m/s (Del Bo et al., 2006) or 37 m/s (Sivakumar et al., 2005) in select patients. In this regard, the mouse phenotype is more severe than the human disease, but whether that represents a more profound loss of large-diameter axons or whether the analysis of the mice was done at a later stage of the disease is unclear.

In the mouse model, sensory nerves are also clearly affected, although this remains ambiguous in the human

disease. CMT2D and SMA-DV are allelic (Sambuughin et al., 1998), but the clinical diagnosis of CMT2D depends on the presence of sensory symptoms. In the five pedigrees initially identified, three presented with purely motor SMA-DV, one with CMT2D, and one was ambiguous (Dubourg et al., 2006; Sivakumar et al., 2005). A sixth pedigree recently reported also has variable sensory involvement (Del Bo et al., 2006). However, even in the mouse, sensory-axon loss had a milder initial severity and less progression than motor-axon loss. If this is also the case in humans, it may contribute to discrepancies in the clinical diagnosis of SMA-DV and CMT2D.

Genetic Background and Allelic Variability

The differences in clinical presentation in CMT2D patients suggest allelic variability in the phenotype. In addition, variability in symptoms such as sensory involvement and age of onset even within pedigrees suggests possible modifier loci in the genetic background may also influence the phenotype. Results in the mouse support both the influence of genetic background and allelic variability. *Gars*^{*Nmf249*/+} mice in a mixed B6/BALB/CAST background exhibit better survival than inbred B6 *Gars*^{*Nmf249*} mice, although they still show overt neuromuscular dysfunction with a similar age of onset. It remains to be determined whether this suppression is caused by a few specific loci or can be attributed to general "hybrid vigor."

In addition to the P278KY mutation of *Gars*^{*Nmf249*} described here, a second allele of *Gars* that also causes dominant neuromuscular dysfunction in mice has been identified in the Harwell Mutagenesis Program in the U.K. (Elizabeth Fisher, personal communication). This new allele has a milder phenotype than the *Gars*^{*Nmf249*} allele, with no early lethality and detection of mutants by grip strength assays, since the locomotor abnormalities are more subtle. This allele is also sensitive to genetic background, producing live-born homozygous pups that survive for days to weeks in some backgrounds while causing embryonic lethality in others.

Thus, though the phenotype of the mouse allele described here is in some ways more severe than the human disease, results in other genetic backgrounds and in other alleles indicate that mouse *Gars* mutations will provide important mechanistic and phenotypic insights into CMT2D pathogenesis.

A Pathogenic Function for the Mutant Protein

The comparable activity of mutant and wild-type GlyRS proteins makes a loss-of-function mechanism through impaired enzymatic activity unlikely. Other defects, such as in vivo instability of mutant homo- or heterodimers or decreased efficiency of protein folding, may account for the slight reduction in GlyRS activity observed in tissue extracts from *Gars*^{*Nmf249*/+} mice compared to controls, though the observed effect is not statistically significant. However, the lack of a dominant phenotype in the *XM256* gene-trap allele, despite significantly lower GlyRS activity in *Gars*^{*XM256*/+} tissue homogenates compared to *Gars*^{*Nmf249*/+} homogenates, eliminates the possibility that the disease is caused by a loss of the canonical GlyRS activity or by a dominant-negative activity of the mutant protein. These

results support the hypothesis that the phenotype is caused by a novel pathogenic function of the mutant protein.

In this regard, *Gars*/CMT2D is analogous to diseases like amyotrophic lateral sclerosis (ALS), caused by mutations in *SOD1*. In each, the loss of peripheral neurons with large-diameter axons results from mutations in a ubiquitously expressed enzyme, but enzymatic activity is not correlated with phenotype (Bruijn et al., 2004). Furthermore, in both ALS and CMT2D, the disease appears to require the expression of mutant protein, and not to be caused by a null-allele. Genetically, *SOD1* mutations are closer to true gain-of-function alleles, where the dosage of the wild-type protein does little to alter the phenotype (Bruijn et al., 1998), while the *Gars*^{*Nmf249*} allele fails to complement a loss-of-function allele. However, some of this difference may be caused by the essential activity of GlyRS, while *SOD1* is dispensable. CMT2D and ALS models also show phenotypic similarities, in that NMJs are affected early in the disease (Fischer et al., 2004; Pun et al., 2006), the severity is length dependent and more severe in distal axons, and large-diameter axons are primarily affected. However, CMT2D has no known central nervous system pathology, while ALS also affects upper motor neurons and shows eventual loss of motor neuron cell bodies in the spinal cord. Intriguingly, two mutant forms of *SOD1* that cause ALS in humans and in transgenic mice also bind lysyl-tRNA synthetase (LysRS), while wild-type *SOD1* does not, suggesting that allele-specific interactions with the translational machinery may contribute to the disease (Kunst et al., 1997). However, as in *GARS*, the mutations in *SOD1* that cause ALS are scattered throughout the enzyme, and only the G85R and G93A alleles have been tested for their interaction with LysRS.

Noncanonical Functions of Aminoacyl Transferases

The charging of glycine onto its tRNAs is essential for translation and is the only known function of the GlyRS enzyme. However, noncanonical functions have been demonstrated for other tRNA synthetases (Lee et al., 2004). For instance, a natural, alternative splice fragment of human tryptophanyl tRNA synthetase and a similar natural proteolytic fragment inhibit angiogenesis through interactions with VE-cadherin (Tzima et al., 2005; Wakasugi et al., 2002). Human tyrosyl-tRNA synthetase is naturally split into two active cytokines that regulate the inflammatory response (Wakasugi and Schimmel, 1999). In this instance, two distinct domains of the protein are important for cytokine functions, suggesting at least the possibility for mutations in scattered regions that could be associated with pathologies. Furthermore, glutamyl-prolyl tRNA synthetase is part of a multisynthetase complex which, under the influence of γ -interferon, translocates to the γ -interferon-activated inhibitor of translation complex (GAIT), where it causes gene-specific translational silencing of a proinflammatory protein (Sampath et al., 2004).

Mutations in glycyl tRNA synthetase and the disease CMT2D are analogous to other degenerative neuropathies, suggesting common pathogenic pathways. For example, mutations in human tyrosyl-tRNA synthetase were recently shown to cause dominant intermediate

CMT type C (Jordanova et al., 2006). However, in this instance the authors reported that the CMT phenotype correlated with a reduction in enzyme activity and a dominant-negative role for the mutant protein, suggesting that a defect in protein synthesis may specifically affect neurons. In contrast, a loss-of-function allele of *Gars* showed no dominant phenotype despite significantly lower GlyRS activity levels than in the *Nmf249* allele. Furthermore, the P234KY mutant enzyme studied here showed no loss of aminoacylation activity. (In other work, we found at least one example encoded by a known CMT-associated specific mutant allele of human *GARS* that also had normal enzyme activity [L.A.N. and P.S., unpublished data].) Because one gene encodes both the cytosolic and mitochondrial forms of the protein in mammals (Mudge et al., 1998; Turner et al., 2000), pathogenesis may be caused by mitochondrial dysfunction. However, the loss-of-function gene-trap allele suggests that the CMT phenotype is not associated with decreased GlyRS activity needed for protein synthesis in the mitochondria or cytoplasm. In addition, the CMT phenotype caused by mutations in TyrRS is associated with the cytoplasmic, not the mitochondrial, enzyme (Jordanova et al., 2006), which in the case of TyrRS is encoded by two distinct genes.

Understanding the cell autonomy, the dysfunctional subcellular compartment, and the molecular interactions of the mutant GlyRS protein will be essential for understanding the pathogenesis of CMT2D and offers the possibility of extrapolating these findings to other neurodegenerative conditions that also affect this population of neurons.

Experimental Procedures

Mice

The *Nmf249* mutation arose in the Neuroscience Mutagenesis Facility at The Jackson Laboratory in 2004. The mutation was originally isolated on an inbred C57BL/6J (B6) background; all experiments described used mice with this genetic background. As the mutation is dominant and lethal before mice can be effectively bred, the strain is maintained by ovary transplantation. Ovaries are surgically removed from 3- to 4-week-old affected mice and implanted into NOD.CB17-*Prkdc*^{*scid*/J} recipient females. The recipient females are then bred by standard practices.

Ages and numbers of mice used in histological, physiological, immunocytochemical, and electron microscopy studies are stated in the text and figure legends. Controls were most often unaffected littermates, though in some studies on femoral nerves, conduction velocities, and enzyme activities, strain- (C57BL/6J) and age-matched controls were used.

All animal procedures were carried out using protocols approved by The Jackson Laboratory Animal Care and Use Committee and in accordance with the NIH Guide for the Care and Use of Laboratory Animals.

Genetic Mapping

The *Nmf249* mutation was mapped to chromosome 6 by breeding affected B6 mice (by ovary transplant) to BALB/cByJ (BALB) males to create B6 \times BALB F1 mice. Affected mice from this cross were then backcrossed (again by ovary transplant) to BALB males to create a segregating N2 population. These animals were scored for overt signs of neuromuscular dysfunction, and a whole genome scan using 98 microsatellite markers (*Dmit* markers) spaced approximately every 10 cM across the 19 autosomes was performed on 16 affected and 11 unaffected mice; complete linkage with *D6Mit188* in the central portion of chromosome 6 was found. The genetic interval was narrowed by recombination mapping on an additional 76 N2 mice using additional chromosome 6 MIT markers (*D6Mit183*

[synonymous with *D6Mit354*], *D6Mit384*, *D6Mit316*, *D6Mit71*, *D6Mit188*, *D6Mit361*, *D6Mit132*).

Sequence Analysis

The *Gars* open reading frame was amplified from first-strand cDNA generated from brain RNA from an affected *Nmf249* mouse. The sequence was amplified in three overlapping segments using the following primer pairs: 1F to 1R (CTAGGCGGCGTGCTCATG to CCCAATGAAGTCTGGAAC), 2F to 2R (CTCCCACCACTGGCAAT GAC to CTCACCTCAGCAGCAGCTCC), and 3F to 3R (GCTAGTGCTG GAGTATCTC to CGTCCCTGGATGCAGTCAC). The PCR products were sequenced directly and compared to the C57BL/6J sequence from the mouse genome project (<http://www.Ensembl.org>, NCBI build m33 mouse assembly) and to the sequence obtained from an unaffected B6 mouse from the same colony. An accurate mouse *Gars* cDNA sequence is available with accession number NM180678 (Lang et al., 1996). Double sequence was found in the 2F-2R PCR product in the *Nmf249* cDNA, indicating an insertion or deletion in this part of the gene. As the mutation is dominant and heterozygous, the PCR product was subcloned by Topo-TA cloning (Invitrogen), and individual clones were sequenced to confirm the sequence change. The same approach was used to confirm the mutation in the genomic DNA of exon 7 (intron 6F to intron 7R, GCCTTGTCTGTAACGTTTGCAC to CAAGTTTACCTTTTGTACAGGC). A mutation-specific and wild-type-specific PCR assay was developed (mutation CCAGGCATATTTCTCCATATTT, wild-type CCAGGCATATTTCTCCAGG, both in combination with intron 6F above), and affected mice were confirmed to carry the mutation.

Immunofluorescence of NMJs

Immunofluorescence was performed as described (Burgess et al., 2004; Gautam et al., 1996). For confocal analysis, muscles were frozen in OCT, and 30 μ m thick cryostat sections were mounted on slides and stained to visualize en face junctions. Cocktails of the following primary antibodies were used to visualize nerves: anti-neurofilament (rabbit polyclonal (Sigma) or SM 31 monoclonal (Stemberger Monoclonals), rabbit anti-synaptophysin (Zymed), and mouse anti-SV2 (DSHB). Alexa Fluor 488-conjugated anti-rabbit and anti-mouse secondary antibodies (Molecular Probes) were used. Tetramethylrhodamine-conjugated α -bungarotoxin (Molecular Probes) was used to visualize acetylcholine receptors on the muscle cell surface. Images were collected on a Nikon E600 fluorescence microscope and SPOT-RT camera or on a Leica NT or SP2 confocal microscope.

Occupancy was determined by examining 100 randomly selected NMJs in each muscle. Junctions where the nerve completely overlapped the AChRs on the muscle were defined as fully occupied, NMJs with vacant receptor territory were defined as partially occupied, and AChR plaques with no nerve associated were defined as denervated. In the P7 and P36-P37 mice examined for Figures 2 and S1, nerves were visualized by EYFP fluorescence after mating to the thy1-EYFP-16 transgenic strain (Feng et al., 2000). In other cases, nerves were stained with anti-neurofilament as described above.

Analysis of *Gars* mRNA Levels

RNA from the brain and kidney of mutant and control mice was poly-A⁺ selected, and 2 μ g of each mRNA sample was run on a denaturing gel, blotted, and probed by standard techniques. The *Gars* 1F-1R PCR product described above was used as a probe for the blot in Figure 1, and 2F-2R was used as a probe for the blots in Figure 6. Loading was standardized by reprobing the blots with a β -actin fragment (Figure 1) or *Rpl29* (Figure 6). The hybridization intensity was quantified using a FujiFilm phosphor imager and the associated software, and ratios of *Gars* signal intensity/standard intensity were determined for each lane. The ratios between mutant and control samples were compared to calculate a percent reduction. For example, in the gene-trap analysis, ratios were 0.30 ± 0.01 versus 0.50 ± 0.05 for the three *Gars*^{XM256/+} brain mRNA samples versus control, and 0.091 ± 0.006 versus 0.167 ± 0.014 for samples from the kidney, giving expression levels of 59% and 54%, respectively.

In addition, 5 μ g of each total RNA sample prepared above was reverse transcribed, and the resulting cDNA was used for quantitative PCR analysis. RNA samples were treated with RNase-free DNase1

before reverse transcribing. Two amplicons were used (forward 1 = GGAGCAGATCCTGGAGATTGACT, reverse 1 = CGGAAGCACTC TCCGTTCTTC, and forward 2 = GTGAACAAGACGCCCCACAC, reverse 2 = CCCAGGTAATGTTGCCGTTG) and β -actin was used as an internal control. Each sample was run in triplicate and averaged for each tissue to represent an $n = 1$. The difference in amplification cycle between *Gars* and the actin standard was calculated for each sample (Amplicon 1 brain Δ Ct = 2.18 ± 0.25 versus 1.48 ± 0.44 for mutant versus control, respectively, $p = 0.07$, kidney Δ Ct = 3.50 ± 0.51 versus 2.26 ± 0.25 for mutant versus control, respectively, $p = 0.02$. Amplicon 2 brain Δ Ct = -0.42 ± 0.07 versus -1.10 ± 0.13 for mutant versus control, respectively, $p = 0.001$, kidney Δ Ct = 0.56 ± 0.48 versus -0.14 ± 0.39 for mutant versus control, respectively, $p = 0.12$). The difference in cycle number determined a fold-reduction in *Gars* RNA expression in the *Gars*^{XM256/+} mice (one cycle = 2-fold change, $\Delta\Delta$ Cts = 0.68 and 0.70 for brain and 1.24 and 0.70 for kidney for amplicon 1 and 2, respectively, average = 0.83- or 1.8-fold reduction in *Gars* mRNA). In all samples in both kidney and brain, the *Gars*^{XM256/+} samples showed lower expression of *Gars* than controls. Both amplicons were downstream of exon 2.

Nerve Histology and Electron Microscopy

Tissue was fixed by transcardial perfusion with 2% glutaraldehyde/2% paraformaldehyde in 0.1 M cacodylate buffer. Sciatic and femoral nerves were dissected free and postfixed overnight in the same fixative. Tissue was then processed for plastic embedding and transmission electron microscopy (TEM) by standard procedures. 0.5 μ m sections were also stained with Toluidine blue and examined by light microscopy. TEM images were collected on a Jeol 1230 microscope. Axon diameters of P35 mice were determined from five nonoverlapping 6000 \times fields from each of three mutant and three littermate control samples. In P7 samples, five 6000 \times fields from each of four mutant and three control mice were analyzed. Distances were determined using the associated software. For counts of axons, left and right nerves were taken whenever possible, and counts were averaged so that each n represents one mouse and the average count of the left and right nerve. The total number of myelinated axons in each nerve was counted using light microscopy on Toluidine blue-stained plastic sections.

Muscle Contractile Experiments

Experimental procedures for in situ muscle recordings were adapted from those used previously in the rat (Seburn and Gardiner, 1995). Anesthesia was induced (tribromoethanol 0.2 mg/10 g), and the mouse was intubated and ventilated with a mix of oxygen and isoflurane (0.5%–1.5%) to maintain anesthesia. CO₂ was maintained at 30–40 mm Hg, and body temperature was maintained at $37^\circ\text{C} \pm 1^\circ\text{C}$.

A dorsal incision through the skin and hamstrings of the leg exposed the triceps surae. The achilles tendon was cut and tied with 4.0 surgical silk to a force transducer (Fort 100, WPI). The sciatic nerve was contacted by a bipolar stimulating electrode. Sciatic nerve branches except the MG nerve were transected and crushed proximal to the stimulating electrode. The hindlimb was clamped at the femur and maintained at $37^\circ\text{C} \pm 1^\circ\text{C}$. A unipolar silver ball electrode was placed in contact with the MG muscle and attached to an amplifier for electromyogram (EMG) recordings.

Stimulus voltage was increased until twitch amplitude no longer increased, and then set 50% higher to ensure maximal activation. Muscle length was adjusted to obtain maximal twitch force.

An isometric muscle twitch (Pt) was recorded following a single stimulus (0.02 ms square pulse) delivered to the sciatic nerve. Tetanic contractions were recorded in response to pulse trains delivered at frequencies of 10, 30, 50, 80, 100, and 150 hertz (0.02 ms pulse duration, 1.2 s), with 2 min of recovery between each stimulus. Mice were removed, and nerve conduction distance was measured, and the MG muscle was removed and weighed.

Measures of peak twitch force, twitch time-to-peak (ms) (TPT), and half-relaxation time (ms) (1/2RT) were derived from the isometric twitch trace. The peak amplitude for each tetanic frequency was measured. All force measures were normalized for muscle weight. Electromyograms were rectified and integrated for analysis.

Nerve Conduction Velocities

In separate experiments, conduction velocity of sciatic axons was calculated by measuring the latency of compound motor action potentials recorded in the muscle of the left rear paw (Occhi et al., 2005). Mice were anesthetized with isoflurane (1%–1.5%) and placed on a thermostatically regulated heating pad to maintain normal body temperature. Action potentials were produced by subcutaneous stimulation at two separate sites: proximal stimulation at the sciatic notch and by a second pair of needle electrodes placed distally at the ankle. For recording, a needle electrode was inserted in the center of the paw (active) and a second electrode (reference) was placed in the skin between the first and second digits. Conduction velocity was calculated as [(proximal latency – distal latency)/conduction distance]. Three animals of each genotype were tested.

Statistical Analysis

A two-tailed t test was used to compare between groups unless otherwise noted. The nonparametric Kolmogorov-Smirnov test (K-S test) was used for comparing the distributions of axon morphometrics, and significance was confirmed by nested-ANOVA. A probability value of ≤ 0.05 was used as a limit for declaring statistical significance. All n values used are based on the number of animals in each group. All values are reported \pm standard deviations.

GlyRS Protein Expression and Purification

For expression and purification, sequence-verified human GlyRS cDNA was obtained (Invitrogen), and the P234KY mutation was introduced via site-directed mutagenesis of the wild-type form using the QuickChange site-directed mutagenesis kit (Stratagene, La Jolla, CA) and the following oligonucleotides as primers: P234KY F, 5'-CTTAATGTTCAAGACTTTCATTGGGAAATATGGAGGAAACATGCCTGGGTACTTG-3' and P234KY R, 5'-CAAGTACCCAGGCATGTTCTCCATATTTCCCAATGAAAGCTTGAACATTAAG-3'. Both the wt and P234KY GlyRS forms were subcloned into pET21a(+) (EMD Biosciences, Inc., Novagen, San Diego, CA) to generate a C-terminal His-tagged form. Both forms of GlyRS were overexpressed in *E. coli* BL21-CodonPlus(DE3)-RIL cells (Stratagene, La Jolla, CA). Cells bearing the GlyRS plasmids were grown overnight to saturation, after which 2.5 ml of culture was used to inoculate 2.5 l of LB medium containing 100 μ g/ml of ampicillin. Cultures were incubated at 37°C shaking until they reached an OD₆₀₀ of 0.6, at which time IPTG (Roche, Indianapolis, IN) was added to a final concentration of 200 μ M to induce expression of GlyRS. After briefly cooling on ice, cells were incubated for an additional 5 hr in a 30°C incubator with constant shaking. Cells were harvested by centrifugation, resuspended in lysis buffer containing 50 mM Tris-HCl (pH 8.0), 300 mM NaCl, 25 mM imidazole, 10 mM β -mercaptoethanol, and EDTA-free protease inhibitor cocktail tablets (Roche, Indianapolis, IN). GlyRS proteins were purified under native conditions, bound to a nickel-nitrilotriacetic acid (Ni-NTA) affinity resin (Qiagen, Valencia, CA), washed with lysis buffer, and eluted on a gradient with lysis buffer supplemented with 25–250 mM imidazole. Fractions of the highest purity were pooled, concentrated in a Centrprep YM-30 (Millipore, Bedford, MA), and diluted in 50% glycerol with 2 mM DTT for storage at –20°C. Concentrations were determined by the Bradford assay (BioRad, Hercules, CA) followed by active site titration.

Aminoacylation Assays

Aminoacylation assays were performed at 37°C in a reaction mixture containing 100 mM HEPES (pH 7.5), 20 mM KCl, 2 mM ATP, 4 mM MgCl₂, 2 mM DTT, 20 μ M L-glycine, 4 μ M [³H]-L-glycine, 100 μ M bulk calf liver tRNA (EMD Biosciences, Inc., Novagen, San Diego, CA), and 1–25 nM wild-type or P234KY GlyRS. Reactions were initiated by addition of reaction mixture and tRNA to the enzyme. Aliquots were removed at appropriate time intervals, spotted onto trichloroacetic acid-soaked filter pads, washed, and measured by scintillation counting (Schreier and Schimmel, 1972). Radioactivity measurements from an enzyme-free experiment were subtracted from all experimental data. Each assay consists of six replica trials; assays were performed twice using independently prepared recombinant protein with similar results.

Enzyme Activity Assays from Tissue Homogenates

Brains from five *Gars*^{Nmf249/+}, three *Gars*^{XM256/+}, and four *Gars*^{+/+} mice, P28–P30, were removed and flash-frozen in liquid nitrogen. Homogenates were prepared and cytosolic fractions obtained by spinning lysates at 100,000 \times g. Aliquots were flash-frozen to avoid freeze/thaw-associated problems. Each assay was performed on 30 μ g of total protein, and each sample was assayed in duplicate with three individual data points taken for each assay. Homogenates were assayed for both GlyRS activity and AlaRS activity, which served as an internal standard for the sample. The ratio of these activities for each animal was analyzed. Assays were performed as described for recombinant protein with the following modifications: 300 μ M bulk calf liver tRNA, 12 μ M [³H]-L-glycine or 5 μ M [³H]-L-alanine, and 1 unit of RNasin RNase Inhibitor (Promega). TCA washes were supplemented with 100 mM L-glycine or D,L-alanine.

Identification of Gene-Trap Mice

The XM256 gene-trap allele was obtained from BayGenomics (baygenomics.ucsf.edu). The insertion in the second exon of *Gars* was confirmed by RT-PCR from the embryonic stem cells. The insertion site was identified as being 519 bp downstream of exon 2 in the second intron of *Gars* by PCR from forward primers in the intron and reverse primers in the β -geo construct and sequencing the resulting amplification product. Any transcript generated from the gene-trap chromosome should not encode more than the first 97 amino acids of GlyRS and would be a fusion of *Gars* and the β -geo insertion. Mice were generated from the ES cells by blastocyst injection. The chimeric mice were bred to C57BL/6J mice to generate F1 mice carrying the XM256 insertion. All analysis was performed in these mice and littermate controls not carrying the insertion.

Supplemental Data

The Supplemental Data for this article can be found online at <http://www.neuron.org/cgi/content/full/51/6/715/DC1/>.

Acknowledgments

We thank the scientific services at The Jackson Laboratory, particularly Peter Finger for tissue embedding and electron microscopy, and Lucy Rowe and Mary Barter for genetic mapping. We thank Louise A. Dionne, Kate E. Miers, and Christine M. Wooley in the Neurosciences Mutagenesis Facility for identifying the original deviant mouse, histology assistance, and colony maintenance. We also thank Drs. Susan Ackerman and Jeffery Milbrandt for their comments on the manuscript. This work was supported by U01-NS041215 for the Neurosciences Mutagenesis Facility and by NIH grants NS054154 to R.W.B. and GM15539 and GM23562 and a National Foundation for Cancer Research fellowship to P.S.

Received: April 7, 2006

Revised: August 11, 2006

Accepted: August 23, 2006

Published: September 20, 2006

References

- Aguayo, A.J., Attiwell, M., Trecarten, J., Perkins, S., and Bray, G.M. (1977). Abnormal myelination in transplanted Trembler mouse Schwann cells. *Nature* 265, 73–75.
- Antonellis, A., Ellsworth, R.E., Sambuughin, N., Puls, I., Abel, A., Lee-Lin, S.Q., Jordanova, A., Kremensky, I., Christodoulou, K., Middleton, L.T., et al. (2003). Glycyl tRNA synthetase mutations in Charcot-Marie-Tooth disease type 2D and distal spinal muscular atrophy type V. *Am. J. Hum. Genet.* 72, 1293–1299.
- Berger, P., Young, P., and Suter, U. (2002). Molecular cell biology of Charcot-Marie-Tooth disease. *Neurogenetics* 4, 1–15.
- Buijn, L.I., Houseweart, M.K., Kato, S., Anderson, K.L., Anderson, S.D., Ohama, E., Reaume, A.G., Scott, R.W., and Cleveland, D.W. (1998). Aggregation and motor neuron toxicity of an ALS-linked SOD1 mutant independent from wild-type SOD1. *Science* 281, 1851–1854.

- Brujin, L.I., Miller, T.M., and Cleveland, D.W. (2004). Unraveling the mechanisms involved in motor neuron degeneration in ALS. *Annu. Rev. Neurosci.* **27**, 723–749.
- Burgess, R.W., Peterson, K.A., Johnson, M.J., Roix, J.J., Welsh, I.C., and O'Brien, T.P. (2004). Evidence for a conserved function in synapse formation reveals *Phr1* as a candidate gene for respiratory failure in newborn mice. *Mol. Cell. Biol.* **24**, 1096–1105.
- Court, F.A., Sherman, D.L., Pratt, T., Garry, E.M., Ribchester, R.R., Cottrell, D.F., Fleetwood-Walker, S.M., and Brophy, P.J. (2004). Restricted growth of Schwann cells lacking Cajal bands slows conduction in myelinated nerves. *Nature* **431**, 191–195.
- Del Bo, R., Locatelli, F., Corti, S., Scariato, M., Ghezzi, S., Prella, A., Fagioliari, G., Moggio, M., Carpo, M., Bresolin, N., and Comi, G.P. (2006). Coexistence of CMT-2D and distal SMA-V phenotypes in an Italian family with a GARS gene mutation. *Neurology* **66**, 752–754.
- Dubourg, O., Azzedine, H., Yaou, R.B., Pouget, J., Barois, A., Meiningner, V., Boutellier, D., Ruberg, M., Brice, A., and LeGuern, E. (2006). The G526R glycyl-tRNA synthetase gene mutation in distal hereditary motor neuropathy type V. *Neurology* **66**, 1721–1726.
- Feng, G., Mellor, R.H., Bernstein, M., Keller-Peck, C., Nguyen, Q.T., Wallace, M., Nerbonne, J.M., Lichtman, J.W., and Sanes, J.R. (2000). Imaging neuronal subsets in transgenic mice expressing multiple spectral variants of GFP. *Neuron* **28**, 41–51.
- Fischer, L.R., Culver, D.G., Tennant, P., Davis, A.A., Wang, M., Castellano-Sanchez, A., Khan, J., Polak, M.A., and Glass, J.D. (2004). Amyotrophic lateral sclerosis is a distal axonopathy: evidence in mice and man. *Exp. Neurol.* **185**, 232–240.
- Gautam, M., Noakes, P.G., Moscoso, L., Rupp, F., Scheller, R.H., Merlie, J.P., and Sanes, J.R. (1996). Defective neuromuscular synaptogenesis in agrin-deficient mutant mice. *Cell* **85**, 525–535.
- Hayasaka, K., Himoro, M., Sato, W., Takada, G., Uyemura, K., Shimizu, N., Bird, T.D., Conneally, P.M., and Chance, P.F. (1993). Charcot-Marie-Tooth neuropathy type 1B is associated with mutations of the myelin P0 gene. *Nat. Genet.* **5**, 31–34.
- Ionasescu, V., Searby, C., Sheffield, V.C., Roklina, T., Nishimura, D., and Ionasescu, R. (1996). Autosomal dominant Charcot-Marie-Tooth axonal neuropathy mapped on chromosome 7p (CMT2D). *Hum. Mol. Genet.* **5**, 1373–1375.
- Jordanova, A., De Jonghe, P., Boerkoel, C.F., Takashima, H., De Vriendt, E., Ceuterick, C., Martin, J.J., Butler, I.J., Mancias, P., Papaiozomenos, S., et al. (2003). Mutations in the neurofilament light chain gene (*NEFL*) cause early onset severe Charcot-Marie-Tooth disease. *Brain* **126**, 590–597.
- Jordanova, A., Irobi, J., Thomas, F.P., Van Dijk, P., Meerschaert, K., Dewil, M., Dierick, I., Jacobs, A., De Vriendt, E., Guergueltcheva, V., et al. (2006). Disrupted function and axonal distribution of mutant tyrosyl-tRNA synthetase in dominant intermediate Charcot-Marie-Tooth neuropathy. *Nat. Genet.* **38**, 197–202.
- Kunst, C.B., Mezey, E., Brownstein, M.J., and Patterson, D. (1997). Mutations in *SOD1* associated with amyotrophic lateral sclerosis cause novel protein interactions. *Nat. Genet.* **15**, 91–94.
- Lang, I.M., Chuang, T.L., Barbas, C.F., III, and Schleef, R.R. (1996). Purification of storage granule protein-23. A novel protein identified by phage display technology and interaction with type I plasminogen activator inhibitor. *J. Biol. Chem.* **271**, 30126–30135.
- Lee, S.W., Cho, B.H., Park, S.G., and Kim, S. (2004). Aminoacyl-tRNA synthetase complexes: beyond translation. *J. Cell Sci.* **117**, 3725–3734.
- Mudge, S.J., Williams, J.H., Eyre, H.J., Sutherland, G.R., Cowan, P.J., and Power, D.A. (1998). Complex organisation of the 5'-end of the human glycine tRNA synthetase gene. *Gene* **209**, 45–50.
- Occhi, S., Zamboni, D., Del Carro, U., Amadio, S., Sirkowski, E.E., Scherer, S.S., Campbell, K.P., Moore, S.A., Chen, Z.L., Strickland, S., et al. (2005). Both laminin and Schwann cell dystroglycan are necessary for proper clustering of sodium channels at nodes of ranvier. *J. Neurosci.* **25**, 9418–9427.
- Pun, S., Santos, A.F., Saxena, S., Xu, L., and Caroni, P. (2006). Selective vulnerability and pruning of phasic motoneuron axons in motor neuron disease alleviated by CNTF. *Nat. Neurosci.* **9**, 408–419.
- Roa, B.B., Garcia, C.A., Pentao, L., Killian, J.M., Trask, B.J., Suter, U., Snipes, G.J., Ortiz-Lopez, R., Shooter, E.M., Patel, P.I., and Lupski, J.R. (1993). Evidence for a recessive PMP22 point mutation in Charcot-Marie-Tooth disease type 1A. *Nat. Genet.* **5**, 189–194.
- Sambuughin, N., Sivakumar, K., Selenge, B., Lee, H.S., Friedlich, D., Baasanjav, D., Dalakas, M.C., and Goldfarb, L.G. (1998). Autosomal dominant distal spinal muscular atrophy type V (dSMA-V) and Charcot-Marie-Tooth disease type 2D (CMT2D) segregate within a single large kindred and map to a refined region on chromosome 7p15. *J. Neurol. Sci.* **161**, 23–28.
- Sampath, P., Mazumder, B., Seshadri, V., Gerber, C.A., Chavatte, L., Kinter, M., Ting, S.M., Dignam, J.D., Kim, S., Driscoll, D.M., and Fox, P.L. (2004). Noncanonical function of glutamyl-prolyl-tRNA synthetase: gene-specific silencing of translation. *Cell* **119**, 195–208.
- Scherer, S.S., Xu, Y.T., Messing, A., Willecke, K., Fischbeck, K.H., and Jeng, L.J. (2005). Transgenic expression of human connexin32 in myelinating Schwann cells prevents demyelination in connexin32-null mice. *J. Neurosci.* **25**, 1550–1559.
- Schreier, A.A., and Schimmel, P.R. (1972). Transfer ribonucleic acid synthetase catalyzed deacylation of aminoacyl transfer ribonucleic acid in the absence of adenosine monophosphate and pyrophosphate. *Biochemistry* **11**, 1582–1589.
- Seburn, K.L., and Gardiner, P. (1995). Adaptations of rat lateral gastrocnemius motor units in response to voluntary running. *J. Appl. Physiol.* **78**, 1673–1678.
- Shiba, K., Schimmel, P., Motegi, H., and Noda, T. (1994). Human glycyl-tRNA synthetase. Wide divergence of primary structure from bacterial counterpart and species-specific aminoacylation. *J. Biol. Chem.* **269**, 30049–30055.
- Shy, M.E., Garbern, J.Y., and Kamholz, J. (2002). Hereditary motor and sensory neuropathies: a biological perspective. *Lancet Neurol.* **1**, 110–118.
- Sivakumar, K., Kyriakides, T., Puls, I., Nicholson, G.A., Funalot, B., Antonellis, A., Sambuughin, N., Christodoulou, K., Beggs, J.L., Zamba-Papanicolaou, E., et al. (2005). Phenotypic spectrum of disorders associated with glycyl-tRNA synthetase mutations. *Brain* **128**, 2304–2314.
- Skarnes, W.C., Moss, J.E., Hurtley, S.M., and Beddington, R.S. (1995). Capturing genes encoding membrane and secreted proteins important for mouse development. *Proc. Natl. Acad. Sci. USA* **92**, 6592–6596.
- Skre, H. (1974). Genetic and clinical aspects of Charcot-Marie-Tooth's disease. *Clin. Genet.* **6**, 98–118.
- Suter, U., and Scherer, S.S. (2003). Disease mechanisms in inherited neuropathies. *Nat. Rev. Neurosci.* **4**, 714–726.
- Turner, R.J., Lovato, M., and Schimmel, P. (2000). One of two genes encoding glycyl-tRNA synthetase in *Saccharomyces cerevisiae* provides mitochondrial and cytoplasmic functions. *J. Biol. Chem.* **275**, 27681–27688.
- Tzima, E., Reader, J.S., Irani-Tehrani, M., Ewalt, K.L., Schwartz, M.A., and Schimmel, P. (2005). VE-cadherin links tRNA synthetase cytokine to anti-angiogenic function. *J. Biol. Chem.* **280**, 2405–2408.
- Verhoeven, K., De Jonghe, P., Coen, K., Verpoorten, N., Auer-Grumbach, M., Kwon, J.M., FitzPatrick, D., Schmedding, E., De Vriendt, E., Jacobs, A., et al. (2003). Mutations in the small GTP-ase late endosomal protein RAB7 cause Charcot-Marie-Tooth type 2B neuropathy. *Am. J. Hum. Genet.* **72**, 722–727.
- Wakasugi, K., and Schimmel, P. (1999). Two distinct cytokines released from a human aminoacyl-tRNA synthetase. *Science* **284**, 147–151.
- Wakasugi, K., Slike, B.M., Hood, J., Otani, A., Ewalt, K.L., Friedlander, M., Cheresch, D.A., and Schimmel, P. (2002). A human aminoacyl-tRNA synthetase as a regulator of angiogenesis. *Proc. Natl. Acad. Sci. USA* **99**, 173–177.